Manladan *et al.*
Chinese Journal of Mechanical Engineering (2024) 37:70
https://doi.org/10.1186/s10033-024-01057-x

Chinese Journal of Mechanical Engineering

ORIGINAL ARTICLE

Open Access

Lap-Shear Performance of Weld-Bonded Mg Alloy and Austenitic Stainless Steel in Three-Sheet Stack-Up

Sunusi Marwana Manladan[1,2], Mukhtar Fatihu Hamza[3], Singh Ramesh[4] and Zhen Luo[1*]

Abstract

With the growing interest in utilizing Mg and austenitic stainless steel (ASS) in the automotive sector, joining them together in three-sheet configuration is inevitable. However, achieving this task presents considerable challenges due to the large differences in their physical, metallurgical and mechanical properties. To overcome these challenges, the feasibility of using weld-bonding to join Mg alloy/ASS/ASS was investigated. The nugget formation, interface characteristics, microstructure and mechanical properties of the joints were investigated. The results show that the connection between the Mg alloy and upper ASS was achieved through the combined effect of the cured adhesive and weld-brazing in the weld zone. On the other hand, a metallurgical bond was formed at the ASS/ASS interface. The Mg nugget microstructure exhibited fine columar grains composed predominantly of primary α-Mg grains along with a eutectic mixture of α-Mg and β-$Mg_{17}Al_{12}$. The nugget formed at the ASS/ASS interface consisted largely of columnar grains of austenite, with some equiaxed dendritic grains formed at the centerline of the joint. The weld-bonded joints exhibited an average peak load and energy absorption of about 8.5 kN and 17 J, respectively (the conventional RSW joints failed with minimal or no load application). The failure mode of the joints changed with increasing welding current from interfacial failure via the Mg nugget/upper ASS interface to partial interfacial failure (part of the Mg nugget was pulled out of the Mg sheet). Both failure modes were accompanied by cohesive failure in the adhesive zone.

Keywords Weld-bonding, Resistance spot welding, Austenitic stainless steel, Mg alloy, Failure mode

1 Introduction

Due to advancements in science and technology, along with a growing worldwide concern for climate change and passenger safety, various materials and related manufacturing technologies are currently being developed for use within the automotive industry [1, 2]. This situation has frequently led to increased complexity in designing vehicle structures. As a result, the practice of joining multiple sheets (three or more) is becoming more and more crucial in vehicle manufacturing. This is being done to meet the demands for lighter and more crash-resistant vehicles while keeping costs reasonable. It is especially required in the fabrication of structures such as front rails, A-, B-, C-pillars, crossmember intersections, and the bulkhead to inner wing [3–6].

As a well-established sheet-joining technology in the automotive industry, with several advantages as high speed, ease of automation and low-cost [7–9], the resistance spot welding (RSW) of multiple sheets has been investigated. Many studies have been conducted on the

*Correspondence:
Zhen Luo
lz_tju@163.com
[1] School of Materials Science and Engineering, Tianjin University, Tianjin 3300350, China
[2] Department of Mechanical Engineering, Faculty of Engineering, Bayero University, Kano 3011, Nigeria
[3] Department of Mechanical Engineering, College of Engineering, Prince Sattam bin Abdulaziz University, 11942 Alkharj, Saudi Arabia
[4] Department of Mechanical Engineering, Faculty of Engineering, University of Malaya, 50603 Kuala Lumpur, Malaysia

RSW of different steel grades and Al alloys in three-sheet configuration. For example, Chtourou et al. [5] investigated the mechanical properties of three-sheet RSW welds, which incorporated two sheets of ultra-high strength 22MnB5 steel and one sheet of DX54D steel. Their findings revealed the peak load is influenced by the thickness of the DX54D steel. Zhang et al. [10] investigated the RSW of three austenitic stainless steel sheets with different joint designs. They found that pullout failure is more likely to occur if the two faying interfaces bear the applied load. Wei et al. [11] investigated the nugget formation in RSW of different grades of advanced high strength steels in three-sheet configuration. Their findings revealed that asymmetric nugget is formed due to the differences in thermal conductivities, electric resistance, and melting point of the materials. Li et al. [12], while investigating the nugget growth in RSW of three-sheets of 5052 Al alloy, found that two small nuggets were formed initially at the faying interfaces. These two nuggets then grew along the axial and radial directions to form one large nugget. In yet another study, Li et al. [13] investigated the failure behavior of three-sheet resistance spot welds of 6061-T6 Al alloy, and developed an analytical model to predict the critical button size to ensure pullout failure [13]. The three-sheet RSW poses significant challenges compared to two-sheet RSW. For instance, Pouranvari and Marashi [14] investigated the nugget growth in three-sheet RSW of steel sheets and observed that, due to the additional interfaces, controlling the heat balance is difficult, making it difficult to achieve nugget sizes that would ensure favorable failure mode. Three-sheet RSW was also found to be more sensitive to variation in welding parameters. The difficulties were found to increase when dissimilar material combinations and/or different sheet thicknesses are used.

In response to the challenges encountered in the RSW of three sheets, there has been a renewed interest in employing a combination of adhesives and RSW, commonly known as weld-bonding [15, 16]. Weld-bonding yields joints that exhibit superior performance when compared to those produced using either adhesive bonding or RSW alone. The adhesive application enhances various aspects, including stiffness, static and fatigue characteristics, corrosion resistance, crashworthiness, and damping capacity. Furthermore, with the application of weld-bonding, the number of welds required in vehicle structures can be reduced [15]. Nevertheless, despite the numerous studies reported on the weld-bonding of two sheets with various material combinations, only limited work has been reported concerning the weld-bonding of three sheets. For example, Zhao et al. [16] and Shen et al. [17] employed weld-bonding to join three-sheet stack-up consisting of hot-dipped galvanized 0.8 mm SAE1004, 1.4 mm DP600, and 1.8 mm DP780 steels. The analysis of the nugget formation and weld quality revealed that additional adhesive (Terokal 5089) significantly increased both the dynamic and static contact resistance between the sheets. Therefore, the weld formation began earlier than in the case of RSW, resulting in a larger nugget size under the same welding conditions compared to RSW [17]. Shen et al. [17] further observed that the nugget formation is influenced by the type of adhesive. When compared to Betamate Flex, the use of Terokal 5089 adhesive produced larger nuggets because of the higher contact resistance at the sheets interfaces. Furthermore, Brechelt et al. [3, 15] investigated the weld-bonding of three-sheet stack-ups comprising UHS-steel (22MnB5), HSLA-steel (HX340) and low carbon steel (DX51) with focus on the weldability lobe and process behavior. The results indicate that the weld-bonding process decreased the effective weldability lobe due to the increase in contact resistance by the adhesive. However, the application of preheat current and optimized welding parameters improved the process stability and welding current range.

The studies mentioned above, which were conducted on three-sheet weld-bonding, have clearly shown that the introduction of adhesive changes the process behavior, and the response of various material combinations to the weld-bonding process varies. Consequently, it is imperative to conduct further investigation of the weld-bonding of three-sheet stack-ups of different materials combination used in vehicles manufacturing.

As the lightest structural materials, Mg alloys are an important material for lightweight vehicles manufacturing [18, 19], and joining them to steel in three-sheet configurations is evitable. However, due to the large differences in properties between Mg and steel, three-sheet joining involving Mg and steel is very challenging. The present authors and their co-researchers [20] have attempted to join 1.5 mm AZ31 Mg alloy and 0.7 mm 316L ASS in three-sheet (Mg/ASS/ASS) configuration using conventional RSW. It was found that, while the ASS/ASS sheets were metallurgically bonded together, the Mg alloy sheet separated from them with little or no-load application during lap-shear test. As an alternative solution, the authors successfully applied resistance element welding (REW) to join the Mg alloy/ASS/ASS. However, the REW process involves additional steps of drilling a hole and inserting a rivet. The added rivet in REW process also has the tendency to increase the entire vehicle weight to a certain extent [21, 22]. Therefore, to maximize the potentials of three-sheet weld-bonding, the presents study seeks to explore the possibility of applying it to join Mg/ASS/ASS, which is an important, but difficult-to-join materials combination. The microstructure

and mechanical performance of the joints under lap-shear loading conditions are investigated.

2 Materials and Methods

Mg alloy (AZ31, 1.5 mm thick) and ASS (AISI 316L, 0.7 mm thick) sheets were used as the base materials (BM). The sheets were cut into welding specimens with a length of 100 mm and width 25 mm (AWS D17.2 Standard) [23]. Alcohol was used to clean the specimens, followed by grinding with abrasive paper to remove surface oxides. This process also aimed to enhance the micro-connection between the adhesive and BMs [24].

The adhesive used for the weld-bonding process was Loctite® Hysol E-60HP™. To maintain a relatively uniform initial adhesive thickness, a thin foil (0.2 mm) was affixed to the non-overlapping sections of the ASS and Mg sheets, based on the work of Feng at al. [24, 25]. The adhesive gun was then utilized to apply the adhesive up to the level of the foil, as illustrated in Figure 1.

Immediately after the application of the adhesive, the samples were assembled and welded using a 220-kW medium-frequency DC RSW machine with maximum welding current capacity of 22 kA. Ater conducting a series of preliminary tests, a constant electrode force of 3.6 kN and welding time of 150 ms were used. Meanwhile, the current was varied in the range of 9−14 kA in increments of 1 kA. Immediately after welding, the foils were removed, and the samples were cured at a temperature of 180 ℃ for 30 min in a furnace.

Samples for macro/microstructural analysis were cut from the cross-section of the joints. The specimens underwent standard metallography procedures, including grinding and polishing. The etching process for the ASS side utilized a solution composed of 10 g $FeCl_3$, 30 mL HCl acid, and 120 mL H_2O, while the etchant for the Mg alloy side comprised a solution of 5 g picric acid, 10 mL H_2O, 5 mL acetic acid, and 100 mL ethanol. The macro-morphology was observed using a stereomicroscope

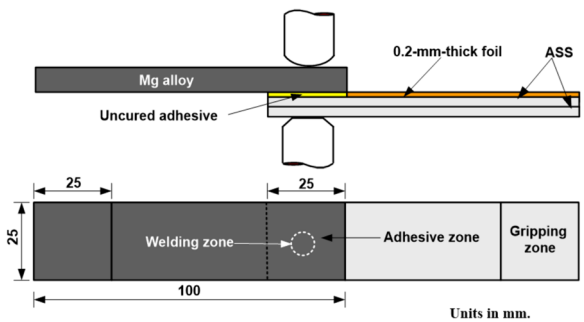

Figure 1 Schematic illustration of the three-sheet weld-bonding process and lap-shear test sample geometry

(Olympus SZX1), while the microstructural analysis was conducted using Olympus GX51 optical microscope (OM). Additionally, the JOEL JSM7600F FESEM (field emission scanning electron microscope) was employed for further characterization of the microstructure, the interface between the Mg nugget and ASS, as well as the fracture surfaces. Energy dispersive spectroscopy (EDS) analysis was conducted to determine the distribution of alloying elements across the joint interface and to measure their concentration on the fracture surfaces.

The hardness distribution across the joint was determined using a micro-hardness tester (Vickers, Huayin HV-1000A) with an applied load of 200 g for 15 s. Lap-shear tests were conducted with a CSS-44100 testing machine at a speed of 2 mm/min. The lap-shear test sample configuration is shown in Figure 1. For each combination of process parameters, three samples were tested. The energy absorption and peak load of the joints were recorded.

3 Results and Discussion

3.1 Macroscopic Morphology and Microstructures

Figures 2(a) and (b) respectively show a schematic illustration and a typical macrostruture of the three-sheet weld-bonded joint. The connection between the Mg alloy and the upper ASS (Mg/ASS1) was established through the combined effect of the cured adhesive and the formed Mg nugget (nugget 1). This nugget resulted from the weld-brazing mechanism, as discussed in the subsequent paragraph. On the other hand, the two ASS sheets (ASS1/ASS2) were joined together by a metallurgical joint at the faying interface (nugget 2). Therefore, as illustrated in Figure 2(a), the nugget size at the Mg/ASS1 interface is denoted as bonding diameter, while the nugget size at the ASS1/ASS2 interface is referred to as the nugget diameter. Under the same welding conditions, the bonding diameter is larger than the nugget diameter. This is discrepancy stems from the significantly lower melting point of the Mg alloy compared to that of the ASS. Hence, while more heat is generated at the ASS1/ASS2 interface due to the higher electrical resistivity of ASS compared to that of the Mg alloy, a higher volume fraction of the Mg alloy would melt compared to the ASS. This resulted in a larger nugget size at the Mg/ASS1 interface.

Owing to the different joining mechanisms at the Mg/ASS1 and ASS1/ASS2 interfaces, these two interfaces are discussed separately as follows.

3.1.1 Mg/ASS1 Interface

As illustrated in Figure 1, the adhesive was applied at the Mg/ASS1 interface, following some preliminary investigations. During the squeeze cycle of the welding process, the uncured adhesive was displaced from the

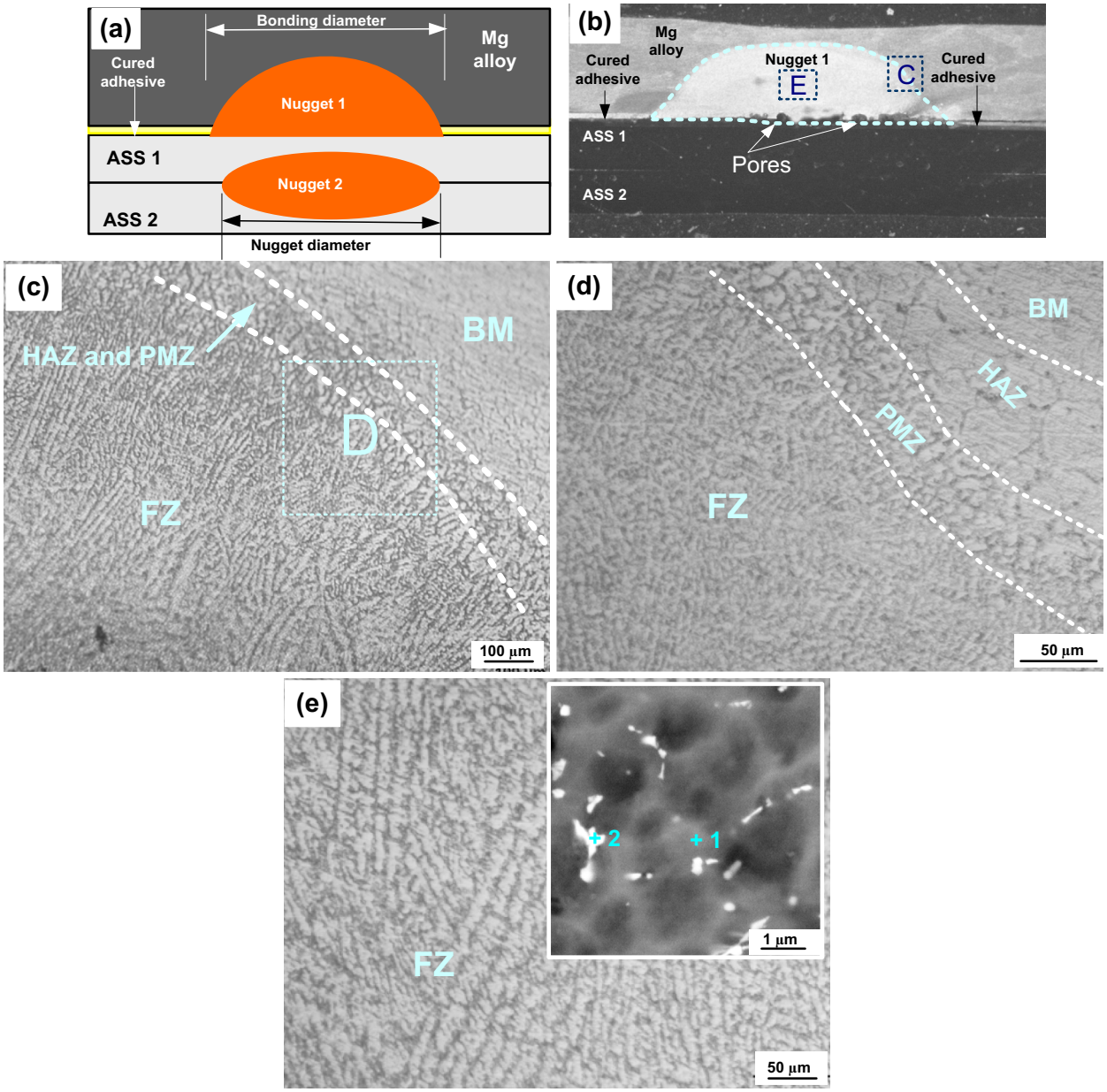

Figure 2 Macrocopic morphology and microstructures: (**a**) Shematic diagram of the joint, (**b**) Macrostructure of the joint, (**c**) Microstructure of area C in (**b**), (**d**) Microstructure of area D in (**c**), (**e**) Microstructure of area E in (**b**)

region under the influence of the electrode force. Therefore, a direct metal-to-metal contact was established at the Mg/ASS1 interface, enabling the flow of welding current across the interface. As the welding current flowed across the interface, Joule heating occurred, causing localized melting of the Mg alloy. The molten Mg alloy then spread and resolidified on the unmelted ASS (weld-brazing), ultimately resulting in the formation of a nugget in the Mg alloy (nugget 1), as shown in Figure 2. It is noteworthy that the Joule heating did not result in the melting of ASS1 at the Mg/ASS1 interface (as can be seen in Figure 2(b)), which would have affected the joint formation, since the melting point of Fe (1450 ℃) is extremely high compared to the boiling point of Mg (1091 ℃) [26, 27]. This can be attributed to the careful selection of appropriate welding parameters and the utilization of asymmetrical electrodes, which enhanced the heat balance across the interface. Furthermore, the Mg alloy functioned as a heat sink for the ASS1 due to its high thermal conductivity, further improving the heat

balance. However, owing to the large differences in physical, metallurgical, and thermal properties between Mg and Fe, several pores were formed near the interface of the Mg alloy and ASS1 within the Mg nugget, as shown in Figure 2(b). The formation of pores in Mg nugget during RSW has been attributed to the followings [28, 29]:

1. The loss of material by vaporization due to the low melting and boiling points of Mg.
2. Rejection of hydrogen during solidification. The solubility of hydrogen in Mg drops drastically during cooling, and thus the dissolved hydrogen in the liquid metal is rejected during solidification, thereby forming pores in the nugget.

Figures 2(c)−(e) show the microstructures of the Mg side of the joint. The microstructure of the Mg BM comprised equiaxed α-Mg grains. However, in the solidified Mg nugget the microstructure consisted of columnar grains. In RSW, columnar grains are typically oriented in the direction of maximum temperature gradient, which corresponds to the direction of electrode compression [30]. The microstructure of the Mg nugget was further characterized using FESEM. The FESEM image (shown as an inset image in Figure 2(e)) shows that some white particles are present in the interdendritic regions of the nugget. To identify these particles, Points 1 and 2 in the figure were analyzed using EDS, and the results are shown in Figure 3. Based on the Mg-Al phase diagram, it can be inferred that Point 1 consisted of α-Mg, and Point 2 consisted of eutectic mixture of α-Mg + β-$Mg_{17}Al_{12}$, indicating that the white particles are β-$Mg_{17}Al_{12}$ particles. Consequently, the nugget microstructure consisted of primary α-Mg grains along with a eutectic mixture of α-Mg and β-$Mg_{17}Al_{12}$. A similar observation was made in the FZ of different resistance spot welded AZ series Mg alloys (AZ80, AZ61, and AZ31) [31]. The β-$Mg_{17}Al_{12}$ particles formation has been attributed to non-equilibrium solidification which lead to the occurrence of eutectic reaction [31, 32].

Referring to Figure 2(d), the Mg nugget is surrounded by a partially melted zone (PMZ). Within this PMZ, which was also observed during the RSW of AZ31 Mg alloy sheets [33], the peak temperature attained was within the solidus and liquidus range of the Mg alloy. Typically, grain boundaries exhibit a higher concentration or segregation of alloying elements/impurities than the interior of grains. This leads to a reduction in their melting temperature relative to the bulk material. Thus, the grain boundaries in the PMZ would experience local melting or liquation as the base metal surrounding the weld is heated. Thus, it represents a transition zone between the completely melted zone (fusion zone) and the completely solid zone (the heat affected zone, HAZ). While the HAZ surrounding the PMZ did not undergo melting, the grains within it experienced coarsening in comparison to those in the BM due to the high temperature experienced in this zone, as shown in Figures 2(c) and (d).

To examine the distribution of major alloying elements at the Mg nugget/ASS1 interface, EDS line scan and elemental mapping were conducted in a region of good connection at the interface. The results, shown in Figure 4, revealed distinct gradients for both Mg and Fe elements at the interface, which is due to the immiscibility of Mg and Fe. Based on the Mg-Fe phase diagram, Mg and Fe exhibit extremely low mutual solubility (< 0.00041 at. %), and no compounds are formed between them [34, 35]. Thus, a metallurgical bond could not be formed between the Mg alloy and ASS1. The Mg alloy would melt and spread on the upper ASS, and nugget 1 was formed (weld-brazing). The occurrence of weld-brazing when joining AZ31 Mg alloy and steel

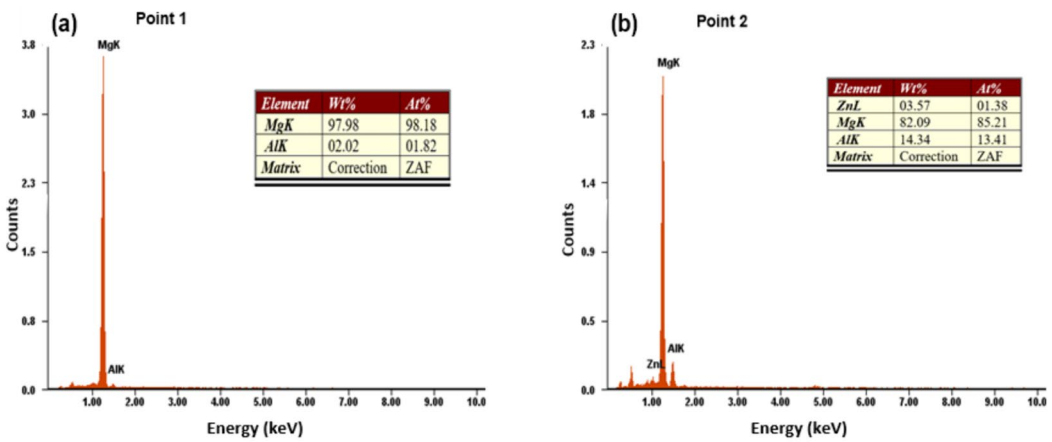

Figure 3 Results of EDS analysis of the points in Figure 2(e): (**a**) Point 1, (**b**) Point 2

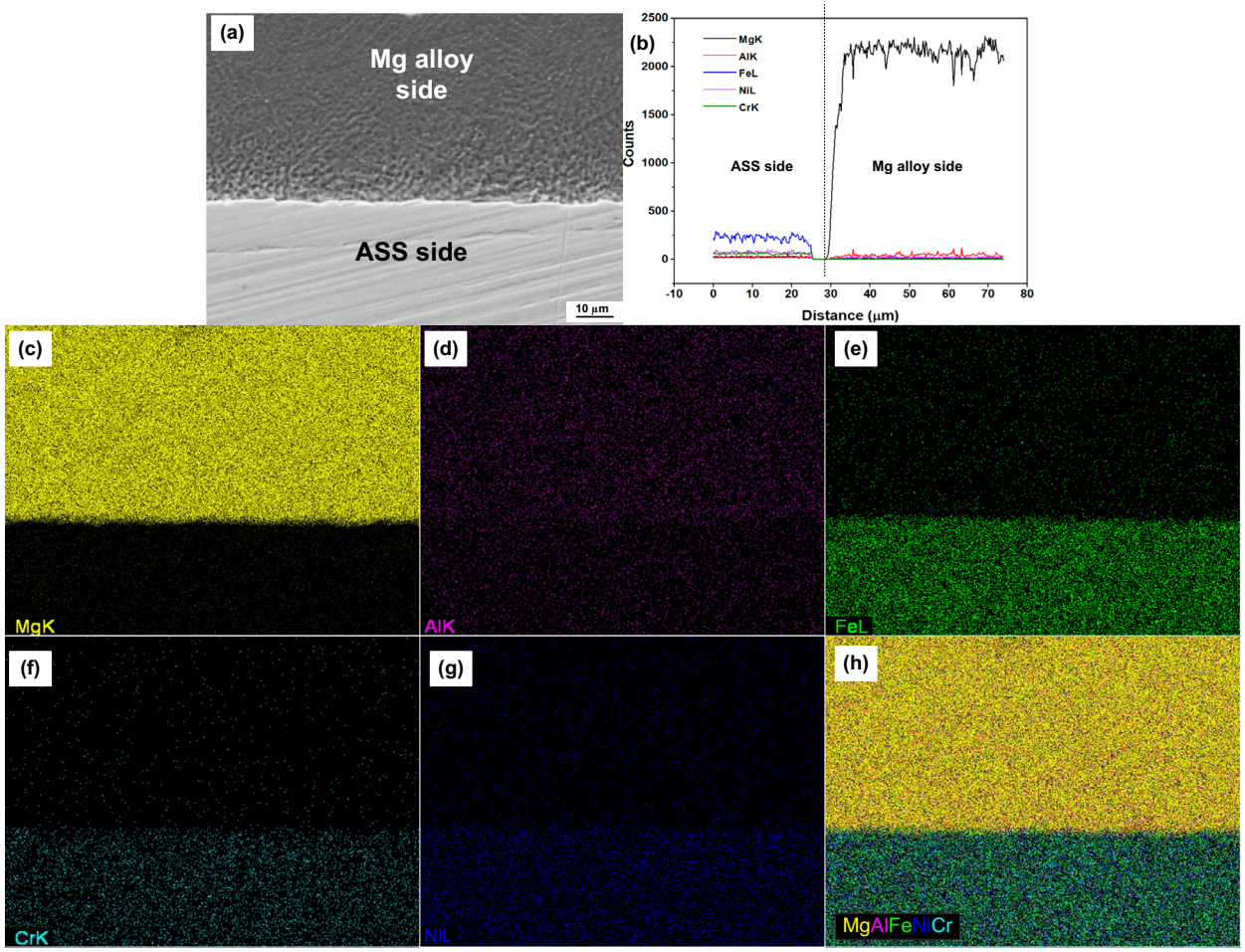

Figure 4 EDS line scan and elemental mapping across the Mg nugget/ASS1 interface: (**a**) SEM image, (**b**) EDS line scan, (**c**)–(**g**) Distribution of elements, (**h**) Overlay distribution

has been attributed to the generation of nano-sized Fe-Al layer on the steel surface [36]. This layer is formed due to the reaction between Fe atoms from the steel and Al atoms from the Mg alloy. Therefore, the melted Mg would spread on the nano-scale layer, subsequently resulting in the formation of the nugget upon solidification.

3.1.2 ASS1/ASS2 Interface

While the weld zone at the Mg alloy/ASS1 interface was formed through weld-brazing, the two ASS sheets (ASS1/ASS2) melted and resolidified at the faying interface, forming a metallurgical bond (nugget 2), as shown in Figure 5. During the RSW of ASS, the single phase austenite present in the BM microstructure undergoes a transformation into a dual-phase microstructure consisting of austenite (A) and delta ferrite (F). The nugget solidification is known to occur in ferrite-austenite (FA) mode, based on the following transformation path [37]:

$$L \rightarrow L + F \rightarrow L + F + A \rightarrow F + A.$$

The F phase is first formed from the liquid (L) phase, followed by the transformation of the A phase from both L and F phases. Under equilibrium conditions, the A phase would gradually consume the F phase through a diffusion-controlled reaction. However, due to the fast cooling rate in RSW, this reaction can not fully complete [10]. Consequently, some F phase would remain in the FZ microstrcuture. As shown in Figure 5(b), the FZ microstructure consisted largely of columnar grains of austenite along with small amount of delta ferrite, elongated parallel to the electrode compression direction. Furthermore, some equiaxed dendritic structures are also observed at the weld center line, as shown in Figure 5(c). According to the solidification model proposed by Kou [38], the ratio of temperature gradient (G) to solidification growth rate (R) governs the transition from columnar to equiaxed

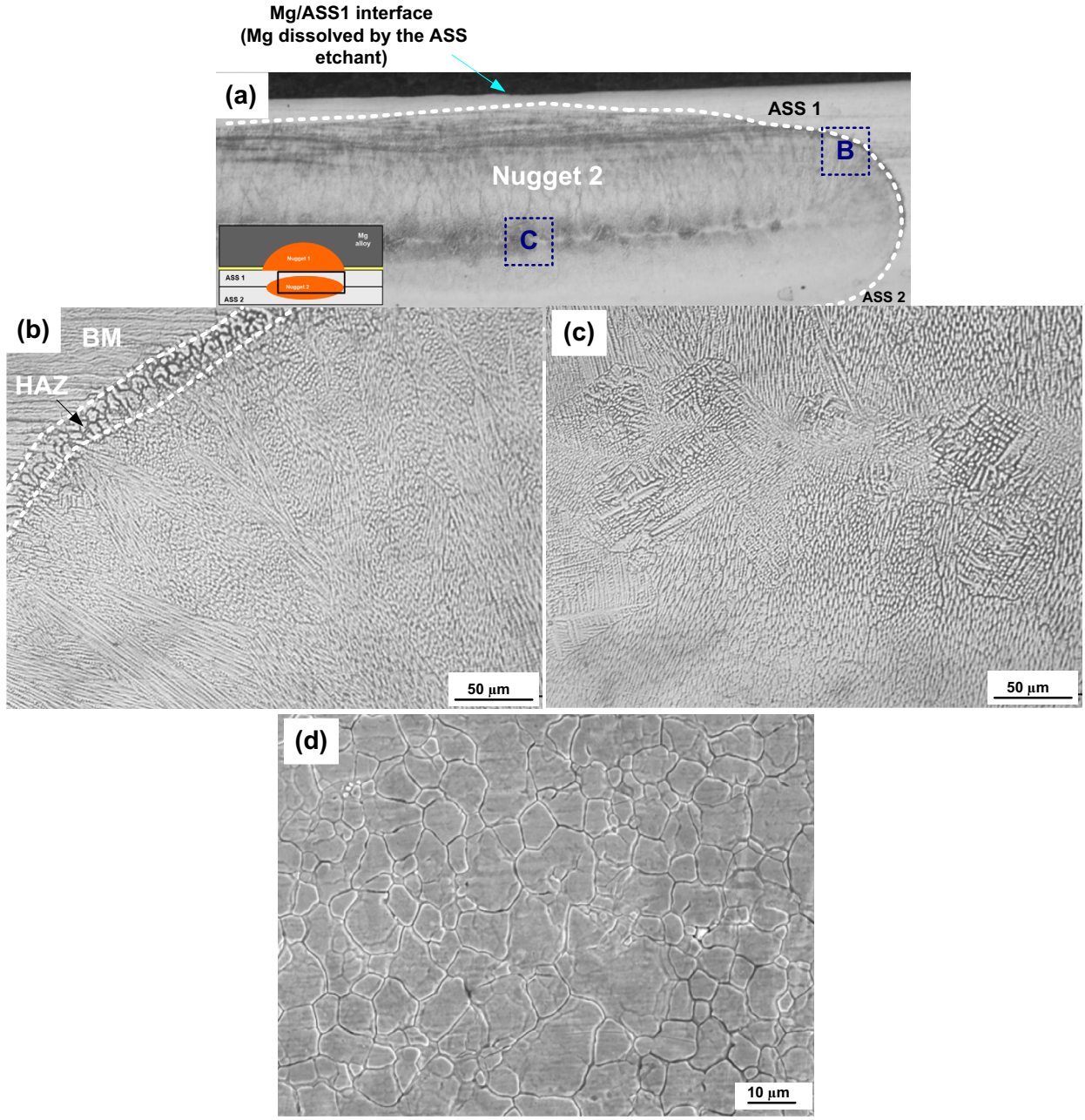

Figure 5 Macro/microstructure of the joint at the ASS1/ASS2 interface: (**a**) Macrostructure, (**b**), (**c**) Microstructures of regions B and C in (**a**), respectively, (**d**) Microstructure of BM

grains (CET). The lower the G/R ratio, the higher the tendency for CET to occur due to higher constitutional supercooling. The formation of equiaxed grains at the center line is due to the higher value R at the solidification front at this location and the lower value of G. The BM microstructure consisted of equiaxed grains (Figure 5(d)). Detailed explanation on the phase transformations that occur during the RSW of ASS can be found elsewhere [39–41].

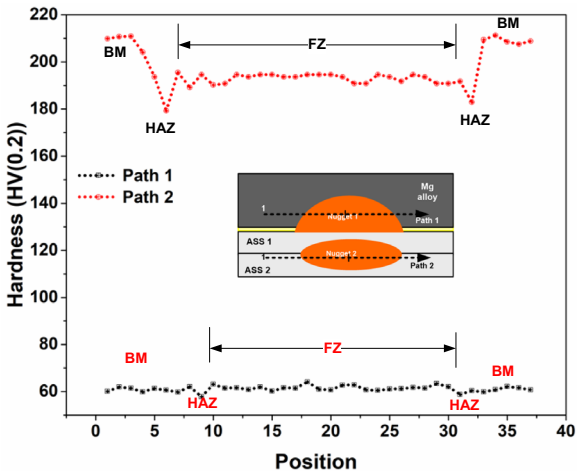

Figure 6 Hardness variation in the joint

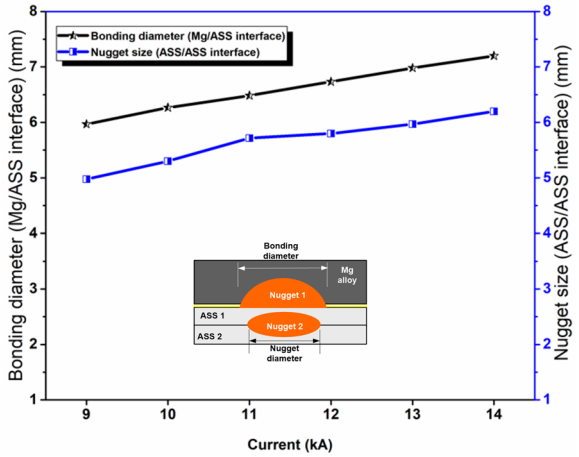

Figure 7 Nugget size vs welding current

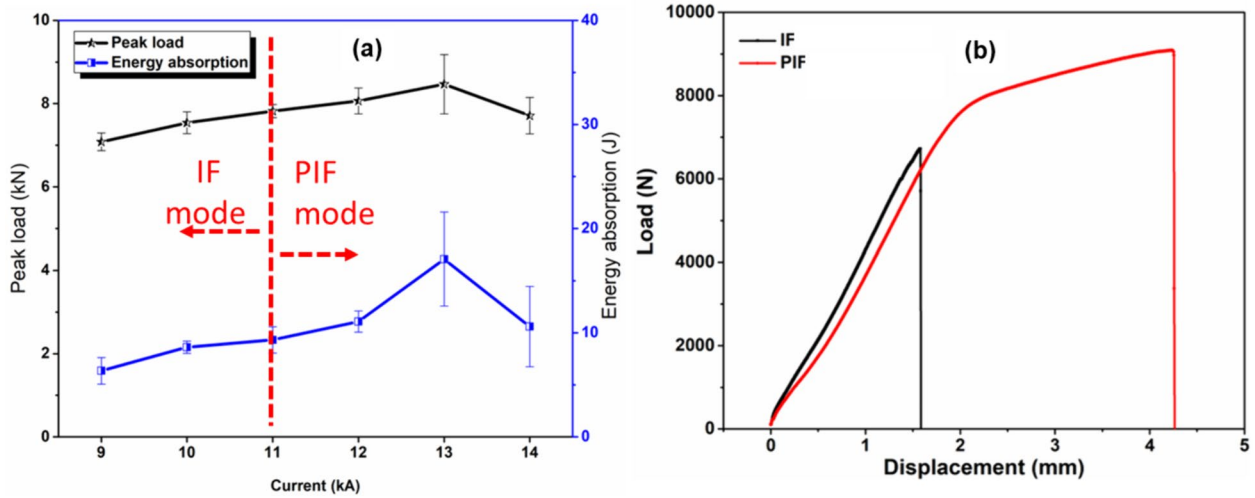

Figure 8 Lap-shear performance: (**a**) Peak load and energy absorption vs welding current, (**b**) Typical L-D curves

3.2 Hardness Variation

Figure 6 shows the typical hardness variation of the joints across two different paths (Paths 1 and 2). Referring to Path 1, only a minor fluctuation in hardness was observed across the Mg nugget and BM. An average hardness value of 61.4 HV and 58.5 HV was obtained for the FZ and BM, respectively. The slight increase in FZ hardness is likely because of the presence of fine columnar crystals (Figures 2(c) and (d). Similar observation was made during the RSW of similar AZ31 sheets [33]. Furthermore, a slight reduction in hardness occurred in the HAZ compared to the BM because of the grain coarsening that occurred in the HAZ relative to the BM (Figures 2(c) and (d)). Referring to Path 2, certain degree of softening can also be observed in the HAZ, which can be attributed to grain coarsening (Figure 5(b)). The FZ hardness is also lower than that of the BM. This observation is consistent with the findings of other authors during the RSW of ASSs [10], and it has attributed to the reduction in prior work hardening effects.

3.3 Lap-Shear Performance

The nugget size is known to be a key parameter that governs the lap-shear performance of spot welds. Generally, the lap-shear performance improves with increasing nugget size. As shown in Figure 7, the nugget size increased with increasing welding current. Accordingly, as shown in Figure 8(a), both the average peak load and energy absorption increased, reaching a maximum value of about 8.5 kN and 17 J, respectively at a welding current of 13 kA. This marks a major improvement compared to conventional RSW joints, where the Mg alloy separated from the two metallurgically bonded ASS sheets with minimal or no load application during lap-shear testing. However, when the welding current was increased above

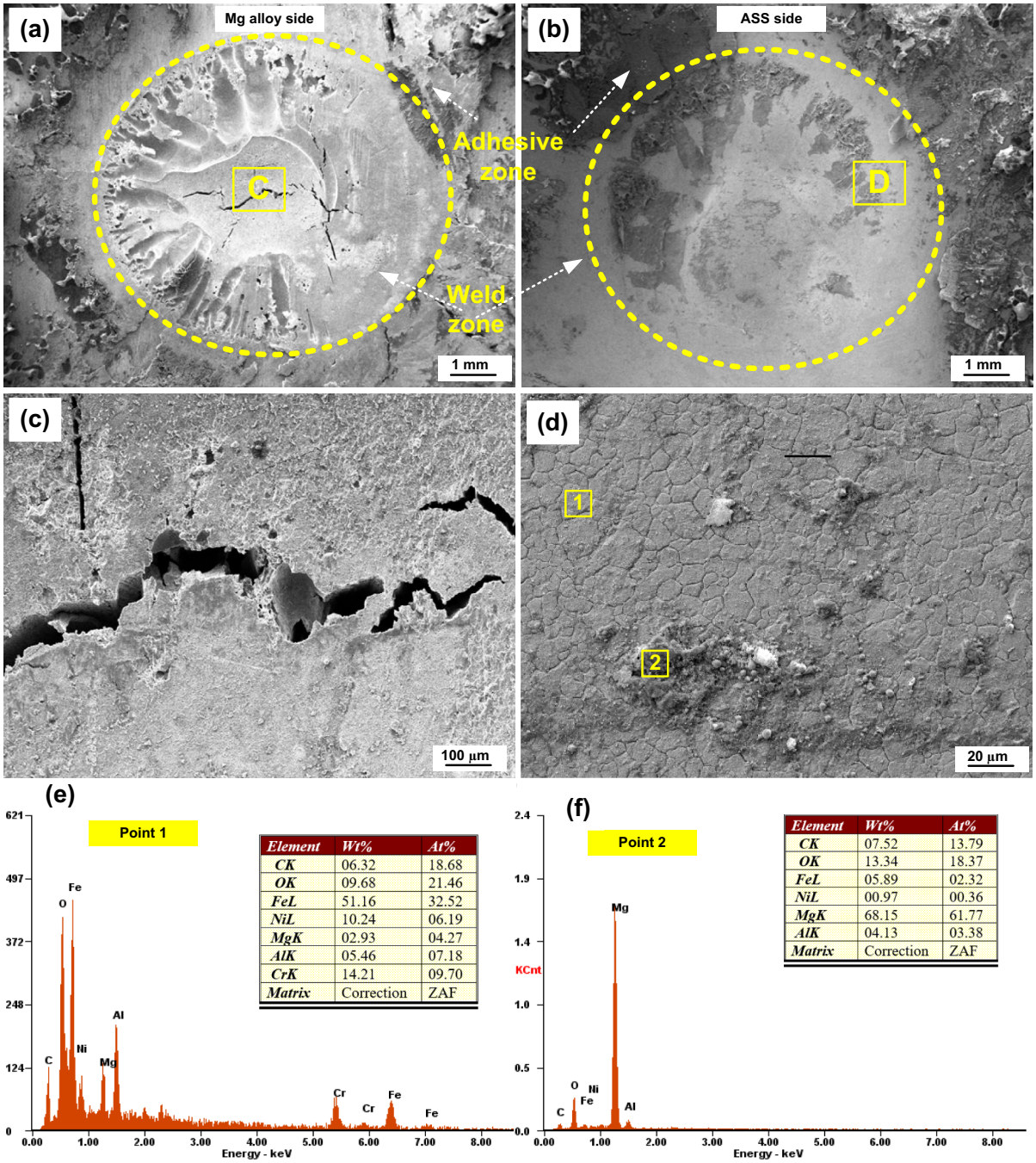

Figure 9 Fracture surface analysis of the joint that failed in IF mode: (**a**), (**c**) Fracture surface of the Mg nugget side, (**b**), (**d**) Fracture surface of the ASS side, (**e**), (**f**) EDS analysis results of areas 1 and 2 in (**d**)

13 kA, both energy absorption and peak load decreased due to the expulsion in the Mg alloy caused by the increased heat generation.

Failure mode is a qualitative measure and a key performance indicator for spot welds [42]. Two types of failure modes occurred in this study: Interfacial failure (IF) and partial interfacial failure mode (PIF) modes. As shown in Figure 7, with the increase in welding current, the bonding diameter also increased, thereby enhancing the joints resistance to IF. As illustrated in Figure 8, the IF mode occurred at the Mg/ASS1 interface within the welding currents of 9–11 kA. The PIF mode occurred at welding

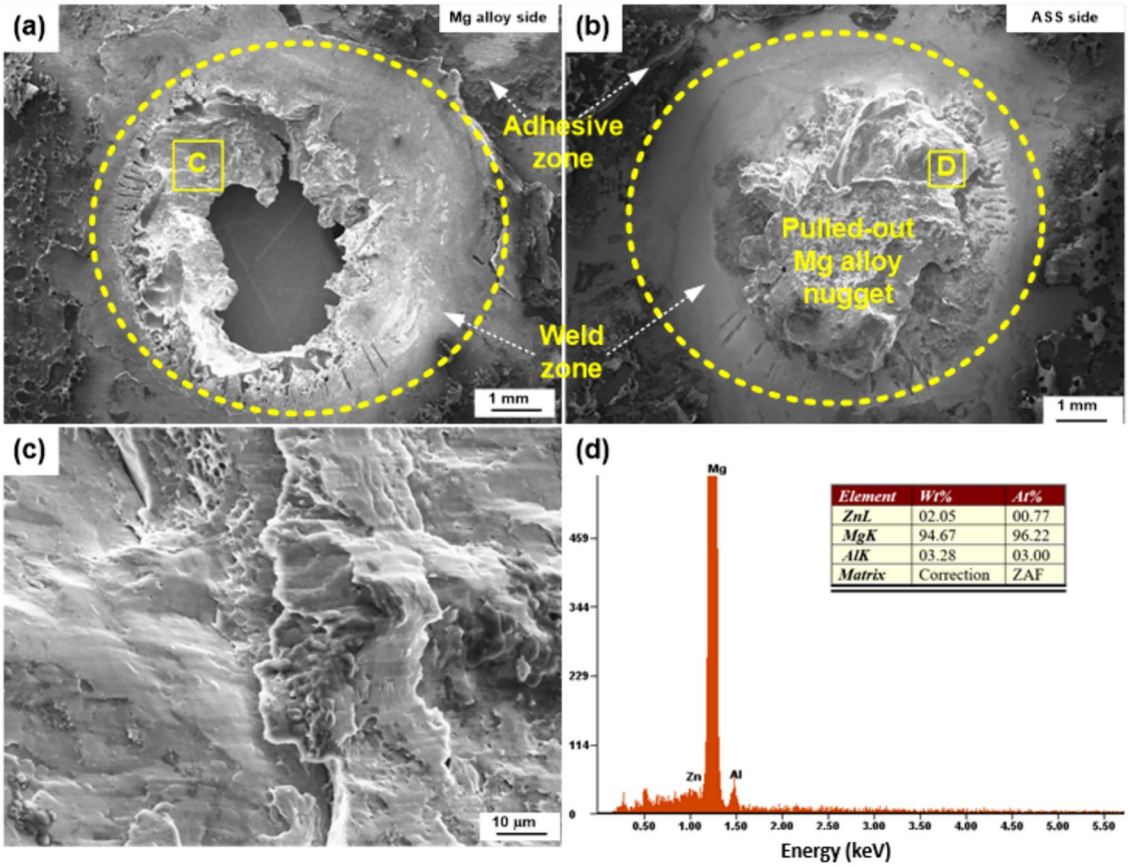

Figure 10 Fracture surface analysis of the joints that failed in PIF mode: (**a**), (**c**) Mg nugget side, (**b**) ASS side, (**d**) Results of EDS analysis of region D in (**b**)

current of 12–13 kA, followed by a shift back to the IF mode at 14 kA.

To elucidate these failure modes further, the representative load-displacement (L-D) curves corresponding to each type of failure mode are shown in Figure 8(b). In the case of the joint that failed in IF mode, the L-D curve illustrates a rapid rise in load as both the welding zone and adhesive zone sustained the load. Subsequently, when the peak load was attained, abrupt failure occurred as the Mg alloy sheet separated from the two ASS sheets through the interface. The typical fracture surface morphologies for the IF mode are shown in Figure 9. These surfaces show that the failure occurred through the Mg nugget/ASS1 interface. Several voids (consistent with the observations in Figure 2(b)) and cracks are observed in the Mg nugget, as shown in Figures 9(a) and (c). Upon conducting EDS analysis of regions 1 and 2 on the fracture surface (Figure 9(d)), the results of which are shown in Figures 9(e) and (f), it is apparent that residual adhesive is present. This observation shows that the compete displacement of the uncured adhesive from the weld zone did not occur during the weld-bonding.

The L-D curve corresponding to the joint that failed in PIF mode suggests that the load also increased rapidly as both the weld zone and adhesive zone sustained the load, and then it increased at a much slower rate as part of the Mg nugget is pulled out. A similar failure mode was observed during the ultasonic spot welding of Mg alloy to steel with Sn interlayer [43]. The fracture surface morphologies are shown in Figure 10. A large hole is clearly seen in the Mg nugget where part of the nugget is pulled out, and the pulled-out nugget is seen on the ASS side (as confirmed by EDS analysis, Figures 10(b) and (d)). Higher magnification image of the fracture surface in the pulled-out region (Figure 10(c)) indicates largely cleavage-like flat facets, indicating brittle failure. It is worth noting that while the lap-shear properties of the joints that failed through PIF mode are superior to that of the joints that failed in IF mode, both types of failure occurred abruptly at the final stage. Referring to Figures 9(a), (b) and 10(a), (b), it is apparent that the adhesive zone in both the IF

and PO modes predominantly experienced cohesive failure within the adhesive. Future studies would investigate the crack propagation phenomena in detail and the effect of adhesive placement and joint design on the lap-shear properties and failure modes.

4 Conclusions

The feasibility of using weld-bonding for joining three-sheet stack-up comprising Mg alloy and austenitic stainless steel (ASS) was investigated. The microstructure and mechanical properties of the joints were investigated, and the following key conclusions are drawn:

1) The connection between the Mg alloy and the ASS involved the combination cured adhesive and weld-brazing in the weld zone. Additionally, the two ASS sheets were metallurgically bonded together.
2) The Mg nugget consisted of fine columnar grains of largely primary α-Mg grains and eutectic mixture of α-Mg and β-$Mg_{17}Al_{12}$. The microstructure of the nugget formed at the ASS/ASS interface consisted largely of columnar grains of austenite. Some equiaxed dendritic grains were formed at the centerline of the joint.
3) While the conventional RSW joints failed with little or no load applixation, the weld-bonded joints exhibited an average peak load and energy absorption of about 8.5 kN and 17 J.
4) The failure mode changed from interface failure via the Mg nugget/upper ASS interface along with cohesive failure of the adhesive to partial interfacial failure along with cohesive failure of the adhesive.

Author's Contributions
SM carried out the experiments and wrote the original draft; MH assisted with the manuscript review and editing; SR assisted with results analysis, and manuscript review and editing; ZL assisted with the experimental plan, results analysis and funding acquisition. All authors read and approved the final manuscript.

Funding
Supported by National Natural Science Foundation of China (Grant No. 52075378), Prince Sattam Bin Abdulaziz University of Saudi Arabia (Grant No. PSAU/2024/R/1445)

Data availability
Not applicable.

Declarations

Competing interests
The authors declare that they have no competing interests

Received: 7 February 2023 Revised: 28 May 2024 Accepted: 6 June 2024
Published online: 22 July 2024

References

[1] J Yang, J Oliveira, Y Li, et al. Laser techniques for dissimilar joining of aluminum alloys to steels: A critical review. *Journal of Materials Processing Technology*, 2022, 301: 1-26.
[2] J Naito, R Suzuki. Multi-material automotive bodies and dissimilar joining technology to realize multi-material. *Kobelco Technology Review*, 2020, 38: 32-37.
[3] S Brechelt, P Neef, H Wiche, et al. Spot weld bonding—process behavior of three-sheet steel stack-ups and analysis strategies with online measuring methods. *Manufacturing Review*, 2020, 7(3): 1-8.
[4] Y Sun, H Fujii, S Zhu, et al. Flat friction stir spot welding of three 6061-T6 aluminum sheets. *Journal of Materials Processing Technology*, 2018, 264: 414-421.
[5] R Chtourou, F Chaari, G Haugou, et al. Experimental study of the mechanical strength and the failure of multi-sheet, multi-material spot-welded assemblies under pure and combined loading conditions. *EPJ Web of Conferences*, 2018.
[6] M Pouranvari, S Marashi. Failure behavior of three-steel sheets resistance spot welds: Effect of joint design. *Journal of Materials Engineering and Performance*, 2012, 21(8): 1669-1675.
[7] Z Ling, T Chen, L Kong, et al. Effects of cover sheets on the nugget growth and fracture behavior of resistance spot welded Q&P980 steel joints. *Chinese Journal of Mechanical Engineering*, 2022, 35: 96.
[8] M Huang, Q Zhang, L Qi, et al. Effect of external magnetic field on resistance spot welding of aluminum alloy AA6061-T6. *Journal of Manufacturing Processes*, 2020, 50: 456-466.
[9] M Moghadam, N S Tiedje, M S Choobi, et al. Bonding mechanisms in spot welded three layer combinations. *9th International Seminar & Conference on Advances in Resistance Welding*, Miami, USA, 2016.
[10] Y Zhang, Y Li, Z Luo, et al. Effect of joint design on the failure behaviour of three-stack-up austenitic stainless steel resistance spot welds. *Science and Technology of Welding and Joining*, 2016, 21(6): 484-492.
[11] S Wei, R Liu, D Lv, et al. Weldability and mechanical properties of similar and dissimilar resistance spot welds of three-layer advanced high strength steels. *Science and Technology of Welding and Joining*, 2015, 20(1): 20-26.
[12] Y Li, F Yan, Z Luo, et al. Weld growth mechanisms and failure behavior of three-sheet resistance spot welds made of 5052 aluminum alloy. *Journal of Materials Engineering and Performance*, 2015, 24: 2546-2555
[13] Y Li, Y Zhang, Z Luo, et al. Failure mode transition of triple-thin-sheet aluminum alloy resistance spot welds under tensile-shear loads. *Welding Journal*, 2016, 95: 479-490.
[14] M Pouranvari, S Marashi. Weld nugget formation and mechanical properties of three-sheet resistance spot welded low carbon steel. *Canadian Metallurgical Quarterly*, 2012, 51(1): 105-110.
[15] S Brechelt, H Wiche, V Wesling. Influence of pre-pulse in spot weld bonding of three-sheet steel stack-up. *Welding in the World*, 2019: 1-12.
[16] Y Zhao, Y Zhang, X Lai. Effect of epoxy adhesive on nugget formation in resistance welding of SAE1004/DP600/DP780 steel sheets. *Materials*, 2018, 11(10): 1828.
[17] J Shen, Y Zhang, X Lai, et al. Adhesive placement in weld-bonding multiple stacks of steel sheets. *Welding Journal*, 2012, 91(2): 59-66.
[18] S M Manladan, F Yusof, S Ramesh, et al. A review on resistance spot welding of aluminum alloys. *International Journal of Advanced Manufacturing Technology*, 2017, 90(4): 605-634.
[19] S M Manladan, Y Zhang, S Ramesh, et al. Resistance element weld-bonding and resistance spot weld-bonding of Mg alloy/austenitic stainless steel. *Journal of Manufacturing Processes*, 2019, 48: 12-30.
[20] S M Manladan, Y Zhang, S Ramesh, et al. Resistance element welding of magnesium alloy and austenitic stainless steel in three-sheet configurations. *Journal of Materials Processing Technology*, 2019, 274: 1162972.
[21] S Wang, Y Li, Y Yang, et al. Resistance element welding of 7075 aluminum alloy to Ti6Al4V titanium alloy. *Journal of Manufacturing Processes*, 2021, 70: 300–306.

[22] W Zhang, X Qiu, D Sun, et al. Effects of resistance spot welding parameters on microstructures and mechanical properties of dissimilar material joints of galvanised high strength steel and aluminium alloy. *Science and Technology of Welding and Joining*, 2011, 16(2): 153-161.
[23] AWS. D17.2 Specification for resistance welding for aerospace applications. *American Welding Society*, 2007.
[24] M Feng, Y Li, C Zhao, et al. Mechanical properties and interface morphology of Mg/Al ultrasonic spot weld bonding welds. *Science and Technology of Welding and Joining*, 2016, 21(8): 688-699.
[25] M Feng, Y Chen, D Fu, et al. Fatigue behaviour and life estimation of Mg/Al ultrasonic spot weld bonding welds. *Science and Technology of Welding and Joining*, 2018, 23(6): 487-500.
[26] L Li, C Tan, Y Chen, et al. Comparative study on microstructure and mechanical properties of laser welded–brazed Mg/mild steel and Mg/stainless steel joints. *Materials & Design*, 2013, 43: 59-65.
[27] R Cao, J Chang, Q Huang, et al. Behaviors and effects of Zn coating on welding-brazing process of Al-Steel and Mg-steel dissimilar metals. *Journal of Manufacturing Processes*, 2018, 31: 674-688.
[28] N K Babu, S Brauser, M Rethmeier, et al. Characterization of microstructure and deformation behaviour of resistance spot welded AZ31 magnesium alloy. *Materials Science and Engineering: A*, 2012, 549: 149-156.
[29] H Luo, C Hao, J Zhang, et al. Characteristics of resistance welding magnesium alloys AZ31 and AZ91. *Welding Journal*, 2011, 90: 249-257.
[30] Y Li, Q Zhang, L Qi, et al. Improving austenitic stainless steel resistance spot weld quality using external magnetic field. *Science and Technology of Welding and Joining*, 2018, 23(7): 619-627.
[31] S Niknejad, L Liu, M Y Lee, et al. Resistance spot welding of AZ series magnesium alloys: Effects of aluminum content on microstructure and mechanical properties. *Materials Science and Engineering: A*, 2014, 618: 323-334.
[32] S M Manladan, F Yusof, S Ramesh, et al. Microstructure and mechanical properties of resistance spot welded in welding-brazing mode and resistance element welded magnesium alloy/austenitic stainless steel joints. *Journal of Materials Processing Technology*, 2017, 250: 45-54.
[33] S B Behravesh, H Jahed, S Lambert. Characterization of magnesium spot welds under tensile and cyclic loadings. *Materials & Design*, 2011, 32(10): 4890-4900.
[34] X Fu, K Chen, C Liu, et al. Microstructure and mechanical properties of dissimilar friction stir lap welding between AZ31 Mg alloy and DC01 steel. *Materials Characterization*, 2022, 187: 111870.
[35] J Cheng, X Hu, X Sun, et al. Multi-scale characterization and simulation of impact welding between immiscible Mg/steel alloys. *Journal of Materials Science & Technology*, 2020, 59: 149-163.
[36] X Wang, D Sun, Y Sun. Influence of Cu-interlayer thickness on microstructures and mechanical properties of MIG-welded Mg-steel joints. *Journal of Materials Engineering and Performance*, 2016, 25(3): 910-920.
[37] J C Lippold, D J Kotecki. *Welding metallurgy and weldability of stainless steels*. New Jersey, USA: John Wiley & Sons, Inc. , 2005.
[38] S Kou. *Welding metallurgy*. New Jersey, USA: John Wiley & Sons, Inc., 2003.
[39] M Pouranvari, M Alizadeh, S Marashi. Welding metallurgy of stainless steels during resistance spot welding, Part I: Fusion zone. *Science and Technology of Welding and Joining*, 2015, 20(6): 502-511.
[40] M Alizadeh, M Pouranvari, S Marashi. Welding metallurgy of stainless steels during resistance spot welding part II–heat affected zone and mechanical performance. *Science and Technology of Welding and Joining*, 2015, 20(6): 512-521.
[41] D Kianersi, A Mostafaei, A A Amadeh. Resistance spot welding joints of AISI 316L austenitic stainless steel sheets: Phase transformations, mechanical properties and microstructure characterizations. *Materials & Design*, 2014, 61: 251-263.
[42] M Pouranvari. Fracture toughness of martensitic stainless steel resistance spot welds. *Materials Science and Engineering: A*, 2017, 680: 97-107.
[43] V Patel, S Bhole, D Chen. Characterization of ultrasonic spot welded joints of Mg-to-galvanized and ungalvanized steel with a tin interlayer. *Journal of Materials Processing Technology*, 2014, 214(4): 811-817.

Sunusi Marwana Manladan is currently a senior lecturer at *Department of Mechanical Engineering, Bayero University, Nigeria*. He obtained his Ph.D. degree from *University of Malaya, Malaysia,* in 2017. His research interests include resistance spot welding and resistance element welding of dissimilar materials.

Mukhtar Fatihu Hamza is currently an assistant professor at *Department of Mechanical Engineering, Prince Sattam bin Abdulaziz University, Saudi Arabia*. He obtained his Ph.D. degree from *University of Malaya, Malaysia,* in 2017. His research interests include manufacturing process optimization.

Singh Ramesh is currently a professor at *Department of Mechanical Engineering, University of Malaya, Malaysia*. He obtained his Ph.D. degree from *University of Sunderland, UK,* in 1997. His research interests include materials characterization.

Zhen Luo is currently a professor at *School of Materials Science and Engineering, Tianjin University, China*. He obtained his Ph.D. degree from *Tianjin University, China,* in 2003. His research interests include resistance spot welding (simulation, visualization, and metallurgy).